Oblique radiative shocks, including their interactions with nonradiative polytropic shocks

F. W. Doss, R. P. Drake, and E. S. Myra

Citation: Phys. Plasmas **18**, 056901 (2011); doi: 10.1063/1.3574386
View online: http://dx.doi.org/10.1063/1.3574386
View Table of Contents: http://pop.aip.org/resource/1/PHPAEN/v18/i5
Published by the AIP Publishing LLC.

Oblique radiative shocks, including their interactions with nonradiative polytropic shocks[a)]

F. W. Doss,[b)] R. P. Drake, and E. S. Myra
Department of Atmospheric, Oceanic, and Space Sciences, University of Michigan, Ann Arbor, Michigan 48109-2143, USA

(Received 19 November 2010; accepted 10 February 2011; published online 4 May 2011)

A theory of shocks dominated by radiation energy flux in optically mixed thin-upstream thick-downstream systems, in which the temperature immediately ahead and some short distance behind the shock front are equilibrated by radiation transport, is presented. This theory is applied to determine properties of the normal and oblique radiative shock, followed by applications to interactions when radiative and polytropic shocks are present in the same system. Comparison with experimental data is presented. © *2011 American Institute of Physics*. [doi:10.1063/1.3574386]

I. INTRODUCTION

For very strong shock waves, the increase in temperature across the shock can be great enough that the transfer of heat by blackbody radiation from the hot shocked regions to the cooler upstream material can become the dominant energy flux in the system, resulting in substantial changes to the shock structure and dynamics. This situation has been studied in several contexts, with most analytical and numerical work to date focusing on either the cases where the gas material is optically thick,[1,2] in which line emission occurs under optically thin conditions,[3] or in the even more extreme case in which, in addition to finding that the radiation fluxes dominate over kinetic energy fluxes, radiation pressure also dominates over material pressures in the system.[4]

The radiative shocks of interest in this paper refer to a strongly radiating shock in the optically mixed thin-upstream thick-downstream case. Steady shocks in this regime have been the subject of analytical work by Drake[5] and McClarren *et al.*[6] Similar to the case of completely optically thin radiating shocks, the postshock density is predicted to rise to very high values. This occurs through the loss of energy from the postshock system to the upstream radiation field. The upstream radiation transport forms a radiative precursor which heats the gas upstream of the shock. The gas is heated at the shock front, but then decreases in temperature due to the radiative cooling until it reaches approximately the precursor temperature. This behavior has led to the perhaps misleading term "isothermal shocks" sometimes being applied to radiative shocks with at least one optically thin direction. However, a truly "isothermal" shock lacking the immediately postshock hot region would have a lower net upstream radiation flux than the radiative shocks in the optically mixed case, and a correspondingly lower net compression.

Experiments to produce radiative shocks have been successfully performed on modern laser facilities in gases,[7,8] foams,[9] and clusters,[10] and on pinch facilities.[11] At the OMEGA Laser Facility at the Laboratory for Laser Energetics,[12] experiments have used laser-driven shock tubes to produce optically mixed shocks in xenon at initially atmospheric pressure with shock speeds above 100 km/s at the time of observation.[13,14] These experiments are diagnosed by x-ray transmission radiography, and the postshock density obtained is found to be over 20 times the initial density.

A complication discovered in the radiative shock experiments involves radiation emitted from the shock interacting with the walls of the shock tube upstream of the shock. For sufficiently fast (and therefore hot) shocks, this heat flow will vaporize the shock tube wall material. The tube wall material then acts as a cylindrically converging piston driving a new, radially converging shock into the system.[15] This shock, called a *wall shock*, interacts with the primary shock near the tube walls, causing a deflection of postshock flow which is clearly visible in the x-ray radiographic data of the experiment. This shock is not itself strongly radiative and will be modeled as a shock in a polytropic gas with constant ratio of specific heats. While previous work focused on identifying the wall shock and proposed utilizing its appearance as a diagnostic of overall shock parameters, an analytic theory describing the interaction did not yet exist. The present work provides such a theory which predicts the output of the radiative shock/polytropic shock interaction.

Section II of this paper introduces a modification of the usual derivation for radiative shocks to accommodate corrections in postshock pressure due to changes in ionization with density. Because calculating shock interactions is dependent on equating pressures in different regions, these corrections to ionization are significant for the results. Sections III A and III B develop the analytic model for oblique radiative shocks, which is applied in Secs. III C and III D to situations in which the fluid flow is and is not everywhere supersonic. Sections III E and III F contain work relevant to the laser-driven experiments described above, including a comparison of experimental data to the radiative interaction model.

II. NORMAL RADIATIVE SHOCKS

In this section, we derive the effects of radiative transfer on the shock structure when no radiation escapes downstream of the shock but radiation upstream is sufficient to

[a)]Paper UI2 5, Bull. Am. Phys. Soc. **55**, 331 (2010).
[b)]Invited speaker.

heat upstream flow to the temperature of the downstream flow. Of particular interest to us is the final density achieved by the material. The derivation here parallels those found in Zeldovich and Razier[1] (Chapter 7) and Drake[5] (Chapter 7).

Calculations will be made in the moving frame of a steady shock. We begin with preshock flow parameters of density ρ_0, velocity V_s, pressure P_0, and enthalpy h_0. The jump conditions ensuring conservation of mass, momentum, and energy can be written as

$$\rho_0 V_s = \rho U \tag{1}$$

$$\rho_0 V_s^2 + P_0 = \rho U^2 + P \tag{2}$$

$$\frac{\rho_0 V_s^3}{2} + \rho_0 V_s h_0 = \frac{\rho U^3}{2} + \rho U h + S, \tag{3}$$

where the term S in Eq. (3) describes all energy flux across the shock not convecting with the fluid, such as by radiation or heat-conduction, and ρ, U, h, and P are local density, flow speed, enthalpy, and pressure. These are supplemented by our equation of state, $P = \rho R(1+Z)T$, where Z is the average particle ionization, $R = k_B N_A/\mu$, k_B is the Boltzmann constant, N_A is the Avogadro number, and μ is the molar mass of the gas species. For such an equation of state, $h = \gamma P/(\rho(\gamma-1))$, where γ is the ratio of specific heats. We may solve these equations to achieve

$$S = \frac{1}{2}\rho_0 V_s^3 \left(1 + \frac{2P_0\gamma}{\rho_0 V_s^2(\gamma-1)}\left(1-\frac{\rho_0}{\rho}\right) - \frac{2\gamma\rho_0}{(\gamma-1)\rho} + \frac{(\gamma+1)}{(\gamma-1)}\left(\frac{\rho_0}{\rho}\right)^2\right), \tag{4}$$

which is a general expression for the evolution of flow parameters beyond the initial state in terms of the nonhydrodynamic flux S, at any later point where the flow has achieved density ρ. Progress is made by assigning $S = 2\sigma T_f^4$ (an approximation for the optically mixed thick-thin case due to Drake[5]), where σ is the Stefan–Boltzmann constant, T_f will be the final downstream temperature achieved by radiation transport, and S is the net radiation from the optically thick postshock region escaping to infinity on the optically thin side. Details of determining the value of S to higher accuracy by solving transport equations can be found in McClarren *et al.*[6] Other models or regimes of radiative shocks may have different expressions for S, in particular the "isothermal" shock with no hot region immediately postshock with $T > T_f$ would have $S = \sigma T_f^4$ without the factor of 2.

With reference to the final state achieved by the fluid, with density ρ_f, temperature T_f, and ionization Z_f, we write the momentum jump condition in Eq. (2) as

$$\eta\left(V_s^2 + R(1+Z_0)T_0\right) = \eta^2 V_s^2 + R(1+Z_f)T_f, \tag{5}$$

where $\eta = \rho_0/\rho_f$ and Z is a function of both T and ρ on each side of the jump. We assume that strong radiation transport will equilibrate the final temperature of the downstream fluid with that of the upstream fluid, $T_f = T_0$ (this is approximately correct through the effect of the total radiation flux on heating of an optically thin precursor; see Drake[5]). Equation (5) now can be solved for the final temperature in terms of shock velocity,

$$T_f = \frac{V_s^2}{R}\frac{\eta(1-\eta)}{1+Z_f-\eta(1+Z_0)}. \tag{6a}$$

Making these substitutions and letting $\rho = \rho_f$ in Eq. (4), we can then write

$$2Q\eta^4\left(\frac{1-\eta}{1-\epsilon\eta}\right)^4 + \eta^2 - 1 = \frac{2\gamma}{\gamma-1}\left(\frac{\epsilon-1}{1-\epsilon\eta}\right)(1-\eta)\eta$$
$$\text{where } Q = \frac{2\sigma V_s^5}{\rho_0 R^4(1+Z_f)^4}, \quad \epsilon = \frac{1+Z_0}{1+Z_f}. \tag{6b}$$

Equation (6b) reduces to a biquadratic equation in η when $Z_0 = Z_f = Z$, and its solutions do not generally deviate far from $\eta \approx (2Q)^{-1/4}$.

We also require an equation of state yielding ionizations ahead and behind the shock,

$$Z_0 = \mathrm{TF}(T_f, \rho_0) \tag{6c}$$

$$Z_f = \mathrm{TF}(T_f, \rho_0/\eta), \tag{6d}$$

TF( ) represents a suitable ionization model, such as Thomas–Fermi,[5,16] evaluated as a function of plasma temperature, density, and (implicitly) ion species. We use here the semianalytical model developed by More and Salzmann.[17,18] Armed with such an ionization model, Eq. (6) forms a complete system of nonlinear algebraic equations which may be solved numerically to obtain self-consistent solutions for given ρ_0, V_s, and ion species. For example, with upstream xenon gas with density $\rho = 0.006$ g/cm^3, $\gamma = 5/3$, and shock speed $V_s = 110$ km/s, we obtain $Q = 2.0\cdot 10^6$, $Z_0 = 13$, $Z_f = 9$, $\epsilon = 1.4$, $T_f = 38$ eV, and $\eta = 1/44$.

A counterintuitive consequence of the lowering of ionization in crossing the shock front is that the sound speed $c = \sqrt{\gamma R(1+Z)T}$ will actually *decrease* across the radiative shock by a factor of $\sqrt{(1+Z_f)/(1+Z_0)}$. This is not a typical behavior across a shock. Another result to note is that, given that the temperature remains constant at $T_f = T_0$, the pressure $P = \rho R(1+Z)T$ will increase across the shock by a factor of $1/\eta\cdot(1+Z_f)/(1+Z_0)$. In the xenon system discussed above, this ratio is lower than the uncorrected value $1/\eta$ by, at high velocities, approximately 30%. Incorporating this effect is essential in the following to generating proper shock polars in pressure-deflection space.

III. OBLIQUE RADIATIVE SHOCKS

A. Oblique shock relations

In the theory of oblique shocks in polytropic media without radiation, the passing of flow through the shock is completely described by the flow's incoming Mach number and the angle β at which the flow meets the shock. For a flow passing from state 1 to state 2, deflected through an angle θ, the relations by which one finds the postshock deflection angle, Mach number M, pressure, density, and speed of sound are well-known to be[19,20]

$$\theta = \tan^{-1}\left(\cot(\beta)\frac{M_1^2\sin^2\beta}{1+\left(\frac{1}{2}(\gamma+1)-\sin^2\beta\right)M_1^2}\right) \tag{7a}$$

$$M_2 = \csc(\beta-\theta)\sqrt{\frac{M_1^2(\gamma-1)\sin^2(\beta)+2}{2M_1^2\gamma\sin^2(\beta)-\gamma+1}} \tag{7b}$$

$$\frac{P_2}{P_1} = \frac{2M_1^2\gamma\sin^2(\beta)-\gamma+1}{\gamma+1} \tag{7c}$$

$$\frac{\rho_2}{\rho_1} = \frac{\frac{1}{2}(\gamma+1)M_1^2\sin^2(\beta)}{\left(\frac{1}{2}(\gamma-1)M_1^2\sin^2(\beta)+1\right)} \tag{7d}$$

$$\frac{c_2}{c_1} = \frac{\sqrt{(\gamma-1)M_1^2\sin^2(\beta)+2}\sqrt{2\gamma M_1^2\sin^2(\beta)-\gamma+1}}{(\gamma+1)M_1\sin\beta}, \tag{7e}$$

where γ is the polytropic index.

For the radiative shock, the relations for polytropes in Eq. (7) do not apply. Instead, Eq. (6) give a complete account of jump conditions provided that one parameter normal to the shock front is known. Because these conditions define the speed of sound upstream of the shock, the upstream Mach number does not vary simply as a flow approaches a radiative shock at different angles. The material flow velocity V_1 does behave straightforwardly and will be used in place of the Mach number as the governing parameter for the radiative oblique shock relations. The angular deflection of flow through the oblique radiative shock θ is

$$\theta = \tan^{-1}\left(\frac{(1-\eta)\tan(\beta)}{\eta\tan^2(\beta)+1}\right), \tag{8a}$$

where η is now found by solving Eq. (6) for an incoming velocity $V_s = V_1\sin\beta$. Because the temperature ahead and behind the shock is equilibrated by radiative conduction, the pressure jump is found by

$$\frac{P_2}{P_1} = \frac{1}{\eta}\frac{1+Z_2}{1+Z_1} \tag{8b}$$

and the total postshock velocity is

$$V_2 = V_1\sqrt{\eta^2\sin^2(\beta)+\cos^2(\beta)} \tag{8c}$$

under the same conditions for η, Z_1, Z_2.

Figure 1 shows the deflection angle θ as a function of incident shock angle β for both the radiative and polytropic shocks passing through the same incident flow. The radiative shock, due to its high compression ratio, obtains far higher maximum flow deflections than the polytropic shock. We also note that while the polytropic shock is defined only for $\beta > \sin^{-1}(1/M_1)$, the radiative shock polar is defined over all β. In actuality, however, we expect that at some low β the normal component of the flow becomes sufficiently slow that the assumptions of strong radiation transport and thermal equilibrium ahead and behind the shock front are no longer justified. The radiative shock solution should therefore be expected in actuality to approach the polytropic solution for low β. However, for β near normal to the flow, the radiative solutions given here should be accurate.

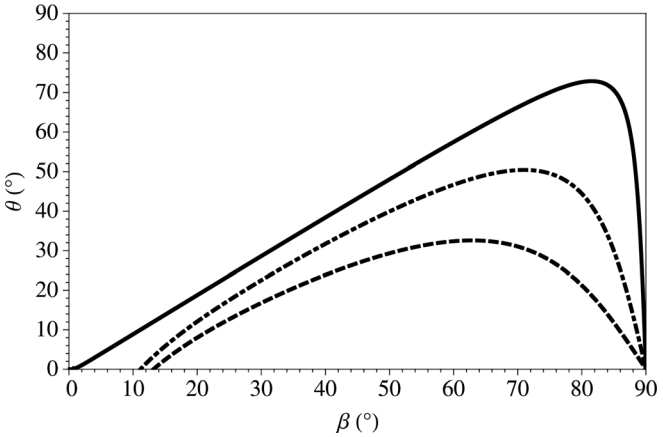

Fig. 1. Flow deflection θ as a function of incident flow β for (solid curve) radiative flow from Eq. (8a) for xenon with $V_1 = 110$ km/s and $\rho_1 = 0.006$ g/cm^3, and polytropic flow from Eq. (7a) with (dashed) $\gamma = 5/3$ at $M = 4.4$ and (dot-dashed) $\gamma = 1.2$ at $M = 5.2$, where the Mach numbers are consistent with 110 km/s in the radiatively preheated case for each γ.

B. Shock polars

A common method of investigating oblique shock effects is to construct shock polars[20] in the space of pressure jump vs. flow deflection, plotting the locus of flow states which can be reached by solving Eq. (7) for all β for which the incoming normal flow is supersonic. We can similarly construct the radiative shock polar by solving Eq. (8).

In systems containing both a radiative shock and a polytropic shock, certain additional rules must be established to obtain a unique solution. We define those rules as follows:

(1) Polytropic shock polars are parameterized by their flow's upstream Mach number, and radiative shock polars are parameterized by their flow's upstream speed.
(2) The speed of sound upstream of a radiative shock is a function of the flow speed normal to the radiative shock. If a region flows into both a radiative shock and a polytropic shock, then the Mach number upstream of the polytropic shock is a function of the angle at which the flow meets the radiative shock.
(3) Flow which passes through a polytropic shock has an immediate postshock sound speed inferred from Eq. (7). This speed may then be used as the incoming speed for a subsequent radiative shock. The density jump must also be calculated and used as the initial condition for the subsequent radiative shock.
(4) Flow which passes through a radiative shock has a postshock Mach number implied by Eqs. (6) and (8), which may then be used as the Mach number for a subsequent polytropic shock.
(5) Each region bound by shocks and discontinuities is bound by at most one radiative shock.

The process of solving systems with these rules is illustrated below in two examples detailing the collision of a radiative and a polytropic shock.

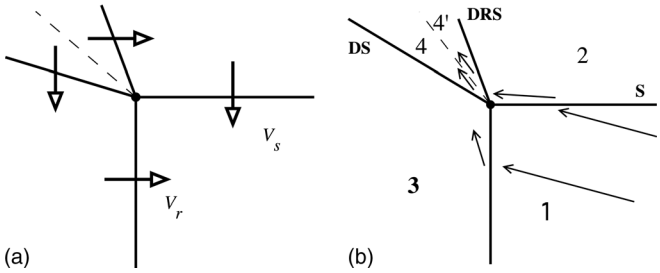

Fig. 2. Schematic for analyzing the four wave intersection (a) in the frame of the upstream gas and (b) in the frame of the point of intersection. Angles are exaggerated. Solid lines indicate shocks: RS, incident radiative shock; S, incident polytropic shock; DRS, deflected radiative shock; DS, deflected polytropic shock. The dashed line indicates a slipstream.

C. Four wave interaction

We consider the four wave interaction shown in Fig. 2(a). In this figure, drawn in the frame of the incident radiating shock, a polytropic shock is advancing orthogonally downward, moving the shock interaction point with it. Figure 2(b) shows the (steady) flow schematic in the frame of the moving interaction point. Because the flow in region 3 is in this frame everywhere supersonic and, therefore, has no information about the incoming polytropic shock, the incident shock does not become curved and the four waves will meet at the interaction point. When the interaction point is steady or subsonic with respect to the upstream system, the topology changes to that with three waves discussed in Sec. III D.

Here and in Section III D, we consider the upstream gas to be xenon at $\rho_1 = 0.006$ g/cm^3 with $\gamma = 5/3$. We consider the initial conditions of, in the frame of the upstream gas in region 1, an incident radiating shock at $V_r = 75$ km/s, and an incident orthogonal polytropic shock advancing at $V_s = 40$ km/s. In the frame of the moving interaction point, this is a flow with velocity $V_1 = 85$ km/s at an angle of 28.1° to the horizontal. The shock polar construction for this flow is shown in Fig. 3.

The flow through from region 1 to region 3 is first solved in order to obtain the sound speed in region 1. We obtain for region 3 flow moving with $\theta_3 = -86.6^\circ$, $V_3 = 40.1$ km/s, and $M_3 = 2.67$. As a check, we verify that $V_3 \sin\theta_3 = -V_s = -40$ km/s, which means that the only velocity in the vertical direction is of the moving frame of the polytropic shock. In the frame of the radiative shock, this is flow entering and exiting the radiative shock normally.

By computing the jump from region 1 to region 3, we also obtain the Mach number of the flow in region 1, $M_1 = 4.24$. It is important in interpreting the Mach number in region 1 to be aware that it refers to the Mach number locally defined in the radiatively heated region immediately upstream of the shock. The Mach number relative to the unheated gas far upstream of the shock would be substantially higher (~480).

Using the solution for M_1, we then pass the flow through the oblique polytropic shock to obtain state 2, in which the flow obtains the values $V_2 = 77.0$ km/s and $\rho_2/\rho_1 = 2.28$. The angles of the deflected shocks are now both unknown parameters, which will be set by the conditions $\theta_4 = \theta'_4$ and $P_4 = P'_4$. We construct in the polar diagram a radiative shock

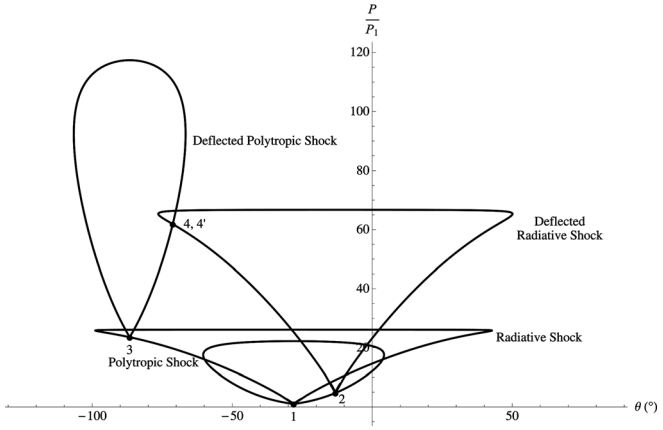

Fig. 3. Shock polars for the four wave interaction.

polar with state 2 as the origin and a polytropic shock polar with state 3 as the origin. Their point of intersection (for the weaker of the two solutions) is $\theta_4 = -71.2^\circ$, $P_4/P_1 = 61.8$. We may also obtain from this analysis such values as the angle of the deflected wall shock with respect to the horizontal (i.e., the incoming flow in the frame of the incident radiating shock). The shock is found to have $\beta = 47.8^\circ$ to move from state 3 to state 4, where $\beta = 90^\circ$ is normal incidence. Taking this angle from state 3, we find that the deflected shock is inclined 38.8° above the horizontal.

We note that performing this calculation correctly in the pressure-deflection space has required the use of the radiative shock polars, particularly in the case of working with state 3, which requires the additional maximum turning angle of the radiative shock. The calculations involving state 3 take place in regions completely inaccessible to the nonradiative shock polars.

D. Three wave interaction

We next consider the case where an oblique polytropic shock intersects a strong radiative shock, shown in Fig. 4. A deflected radiative shock and a slipstream (shear flow boundary) exit the point of interaction, and the system is one of steady flow. Because the flow behind the radiative shock is subsonic to all other interactions in the system, the shock can become slightly curved in the vicinity of the triple-point, eliminating an additional wave from the system.[22] The situation where this was not the case appeared in Sec. III C. Our consideration of this case is heavily influenced by comparison with experiments,[15] in which the nonradiative wall shock intersects the primary radiative shock at an oblique angle. Because the triple-point is steady in these experiments, the flow behind the radiative shock will be subsonic, implying that the observed interaction will be of the three-wave type.

We will specify the upstream flow and angle at which the oblique polytropic shock meets the radiative shock and attempt to predict the downstream flow properties including the flow angle in regions 3 and 3′. The angle of the deflected radiative shock is an unknown parameter in this exercise, and will be calculated from the condition that flow angles and flow pressures must be equal across the slipstream separating regions 3 and 3′.

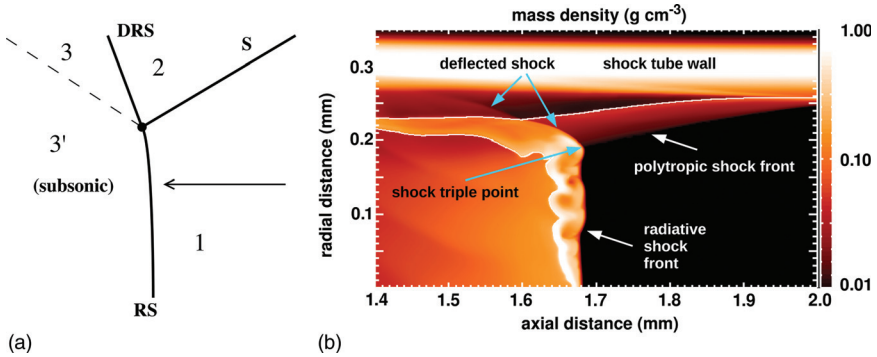

Fig. 4. (Color online) (a) Schematic for analyzing the three wave intersection in the frame of the shocks. Solid lines indicate shocks: RS, radiative shock; S, polytropic shock; DRS, deflected radiative shock. The dashed line indicates a slipstream. (b) A three wave interaction observed in simulations analogous to the experiments referenced in Sec. III F, simulated in the radiation hydrodynamics code CRASH.[21] The shock in the simulation was initiated by a 170 eV x-ray source driving a beryllium ablator to launch a shock into xenon gas at 0.006 g/cm^3. The time shown is 12.0 ns after the x-ray source has been turned off, and beryllium, xenon, and polyimide plastic material interfaces are also present in the region shown.

For initial conditions, we consider the incoming flow to have speed $V_1 = 110$ km/s and to be normal to the lower areas of region 1. We take the angle of the polytropic shock in the system to be 20° with respect to the flow. This number is chosen to produce an angle θ_2 which matches a flow observed behind a nonradiative wall shock in experimental radiography of Omega Shot 52670, discussed further in Sec. III F.

By solving Eq. (6), we obtain a speed of sound in region 1 of 25.1 km/s and an incoming Mach number of 4.38. This calculation also gives us the outgoing speed in region 3′ near the bottom of the figure, which is $V_{3\prime} = 2.47$ km/s, or $M_3' = 0.115$. This will be nearly true throughout region 3′. The flow throughout region 3′ is subsonic.

We return to region 1 and solve the flow through the oblique polytropic shock, using the speed of sound in region 1 found above. Because the angle of the polytropic shock is set, we may find the flow in state 2 directly by evaluating Eq. (8) with $\beta = 20.0^\circ$. We find that $\theta_2 = 8.0°$, $P_2/P_1 = 2.56$, $\rho_2/\rho_1 = 1.71$, and that the flow exits with speed $V_2 = 106$ km/s.

Because the angle of the deflected radiative shock and the curvature of the incident radiative shock are unknown, we must find them through the conditions $P_3 = P_{3\prime}$ and $\theta_3 = \theta_{3\prime}$. This can be done intuitively through the use of shock polars, shown in Fig. 5. To represent passage through the deflected radiative shock, a radiative shock polar is placed with its origin at flow state 2, using the speed and material properties (i.e., density) and speed of state 2. The initial radiative shock polar intersects this deflected polar at $\theta_3 = -14.7^\circ$, $P_3/P_1 = 32.6$. The flow in region 3 is supersonic.

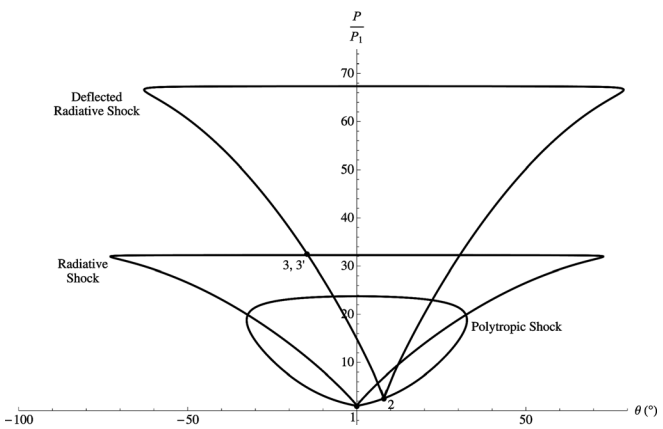

Fig. 5. Shock polars for the three wave interaction.

Once one has obtained the state of region 3 in this method, one may calculate the required curvature of the radiative shock to produce this flow. One finds that the curvature of the radiative shock need only be 0.3°.

In the work by Doss *et al.*[15] which first considered the interaction of radiative shocks with wall shocks, it was assumed that the flow in region 3 was subsonic, based on the observation that the flow avoids impacting into the wall. The calculations in Sec. III D show, however, that there is no subsonic solution for flow in that region. The redirection of flow away from the wall therefore requires additional waves to exist in the system, which motivates the construction described in in Sec. III E.

E. Interaction in the presence of a wall–six wave interaction

This section presents the steady radiative shock–polytropic shock interaction in the presence of a wall. The experimental system to be modeled is a radiative shock with speed V_r launched in xenon gas contained in a polyimide tube with inner diameter 575μm. Introducing the wall into the radiative shock system, we add the following rule to our previous list:

(6) Behind a radiative shock, a wall is a perfect reflecting boundary through which fluid does not pass. Ahead of a radiative shock, a wall is a material source of fluid propagating (in the frame of the wall) perpendicularly away from the wall.

The strong radiative transport upstream of a radiative shock drives an ablation event of wall material, which then flows into the fluid volume, driving the nonradiative, polytropic wall shock into the system.[15] In the frame of the radiative shock, as shown in Fig. 6, the wall shock is formed such that flow passing from region 1 to region 2 travels at the same angle as the flow emitted from the wall (with horizontal component V_r to the left and vertical component V_w downward).

We will in this section neglect the difference in materials emitted from the wall and the gas found in region 1. Furthermore, in regions 1 through 5 we will neglect to consider

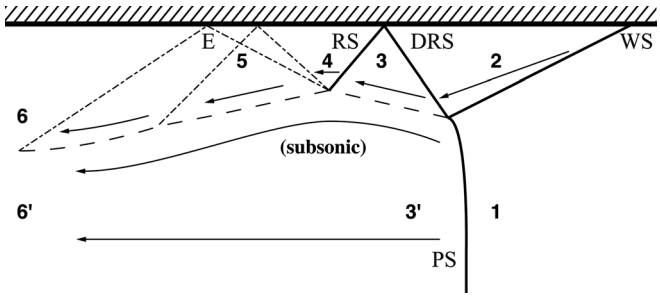

Fig. 6. Schematic of the wave interactions and flow regions in the radiative shock tube experiment. Solid lines represent shocks, the dashed line represents a slipstream, and the dot-dashed lines represent expansion characteristics. PS, primary (radiative) shock; WS, wall shock; DRS, deflected radiative shock; RS, reflected shock; E, expansion region.

the shock tube, an axisymmetric system, treating the area of interest instead as a plane two-dimensional system bounded on the top by a wall and on the bottom by a reflecting boundary condition (*not* a wall). This simplification is justified while the flow remains at large distances from the tube axis. In the transition from region 5 to region 6, this simplification will be discarded.

The upstream material in region 1 is taken to be xenon at 0.006 g/cm^3 with $\gamma = 5/3$ throughout. The speed of the radiative shock V_r is 110 km/s and the speed of the wall shock V_w is 40 km/s (chosen to match $\theta_2 = 8.0$ as measured in Omega Shot 52670). By solving Eq. (6), the Mach number of the fluid in region 1 is 4.38.

The flow begins as in the three wave interaction, passing from region 2 to region 3 through a deflected shock and from region 1 to subsonic region 3′ through the curved portion of the primary shock. As before, the curvature is found to be 0.26°, producing the outward flow at $\theta_3 = \theta_{3\prime} = -14.7^\circ$.

Region 4 is bounded by the wall, behind a radiative shock and therefore not ablating. In order to produce flow parallel to the wall, $\theta_4 = 0$, a shock reflection occurs producing a reflected shock. The system meets the requirement for regular reflection of the shock from the wall, so only one additional shock is required by this interaction.[23] On the polar diagram in Fig. 7, the reflected shock is seen emitting from state 3, containing a state 4 constrained to $\theta_4 = 0$. We find from the intersection of the reflected shock with the ordinate axis $P_4 = 100\,P_1$, with flow locally at Mach 1.9.

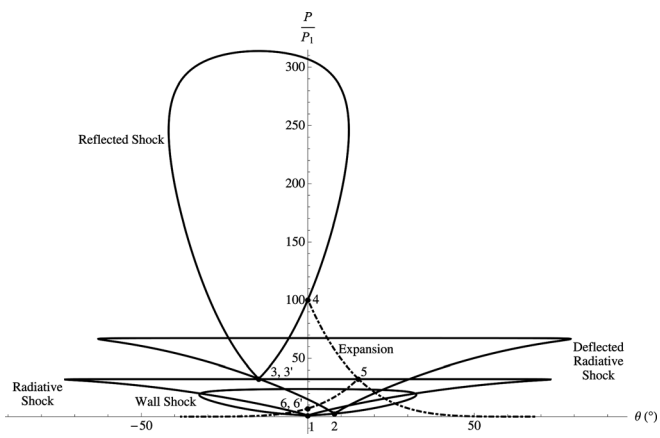

Fig. 7. Polars for the radiative shock tube model.

Following Fig. 6 we then see that the reflected shock intersects with the slipstream separating the region of supersonic flow near the wall with the region of subsonic flow near the center of the tube. Such interactions can in principle be quite complex, but we simplify the analysis to the following conditions. In the supersonic region, some form of wave, separating regions 4 and 5, will be reflected back into the supersonic region. No such standing wave can propagate into the subsonic region, and therefore the pressure there is unaffected by the interaction. The reflected wave then cannot be another shock, which would increase pressure in passing from region 4 to region 5, but must instead be an expansion fan, decreasing the pressure to that in regions 3 and 3′.[24] The direction of streamlines in the subsonic region, however, can change in the vicinity of the interaction, and a kink in the subsonic–supersonic streamline will develop. To visualize this process, we may construct in Fig. 7 a polar representing isentropic expansion of the flow originating in state 4.[20] The Prandtl–Meyer expansion flow which obtains the final pressure $P_5 = P_3$ obtains an inward flow $\theta_5 = -14.7$ (in general close but not exactly equal to the negative of the outward flow angle θ_3).

Finally, our flow's boundary conditions require that its final state (region 6) must be parallel to the wall ($\theta_6 = 0$). This is obtained by realizing that throughout region 5, where the characteristics of the expansion fan meet the wall they must reflect inward.[25] The reflected expansion curves the flow to again be parallel to the wall. While in general more reflections may result between the slipstream and the wall, the characteristics can terminate on the slipstream if the streamline is suitably curved. It will be assumed that the streamline obtains such a shape that no further reflections occur without any attempt to calculate this shape. Treating the passage through the second expansion region as a single isentropic expansion, we see in Fig. 7 that the final pressure is quite low relative to the immediate postshock pressure, $P_6 = (1/4.6)\,P_3 = 7\,P_1$.

We will also approximate the effects in the subsonic region of lowering the pressure to $P_{6\prime}$. Modeling the flow in the subsonic region from region 3′ to 6′ as isentropic flow, we can obtain the final diameter of the initial flow. The xenon flow in region 3′ has a Mach number of 0.1. For additional accuracy, we should regard the xenon as a piston pushing on rarefied beryllium expanded from the laser-absorbing ablator which launched the system, with speed and pressure equal across the material discontinuity. Under these conditions, the beryllium in state 3′ has a Mach number of 0.05. Given the inner diameter of the tube is 575 μm, with 60 μm around the outside of the tube given to the wall shock and the supersonic region, one finds that to reduce the beryllium pressure from P_3' to P_6' requires contraction of the subsonic region to a diameter of 140 μm, and that the "subsonic" region has actually reaccelerated to a Mach number of 1.4 in obtaining region 6.

F. Comparison with data

Experimentally, the interface between shocked xenon and ablated wall material may be used as an optical tracer to image the various angles predicted by this analysis. Regions

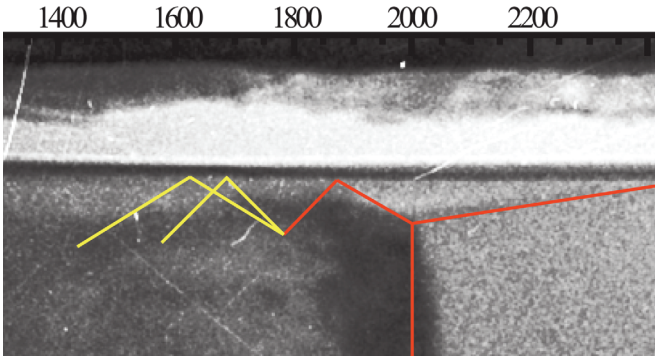

Fig. 8. (Color online) Schematic illustration of the wave interaction scheme presented in Sec. III E overlaid on data from Omega Shot 52670,[13] imaged at 13 ns from the beginning of the drive. Red lines indicate shocks, yellow lines indicate expansion waves. The numbers show distance from the shock tube drive's initial location (in micrometer) and provide both horizontal and vertical scale.

1 through 5 are reliably visible in the experimental radiographs as regions of approximately unbent flows directed outward, parallel to the wall, and then inward. We consider data from the experimental campaign described in Doss *et al.*[13] Figure 8 shows a partial image obtained in this series of experiments. Although this campaign was launched with nominally identical targets, variations in the target construction and initial conditions create some variations in output. In shock data with good signal-to-noise, the boundary between ablated tube wall material and upstream xenon is detectable, which can be used as a measurement of θ_2, the angle of flow in region 2. The flow in region 3, θ_3, is measurable as the interface between dense postshock xenon and transmissive upstream material. The theory in Sec. III D can then be used to predict the flow in region 3 as a function of the flow in region 2, shock speed, and ratio of specific heats, $\theta_3(\theta_2, V_r, \gamma)$. In the experiment, the ratio of specific heats γ for the xenon will be lower than 5/3, due to the effects of ionization.[26] Using the upstream Mach number calculated for a given V_r using the relations in Sec. II, the calculations can be repeated with an entirely nonradiative model using polytropic shocks. Figure 9 plots radiative and nonradiative predictions for θ_2 vs. θ_3 along the measured data. Five of the six images with unambiguous measurable wall shocks support the radiative model. Where the data do not agree with the prediction, it is likely that the assumption of either approximately steady or approximately axisymmetric flow has been violated, either locally in the area of measurement or globally across the shock. This could be a consequence of instabilities which have been associated with radiative shocks.[27–29]

Measurement beyond region 3 is in general complicated, as in the experiment the shock tube wall begins to explode outward after the deflected shock reaches the tube. Measuring region 6 suffers additional difficulties, including that at early times the supersonic xenon may not have reached the end of region 5 (the assumption of a steady system has not been achieved). All measurements are subject to difficulties such as three-dimensional effects in the initial condition (i.e., nonplanar primary shocks). Nevertheless, the qualitative visible signature of the data is that of the system presented in Sec. III E, Fig. 8.

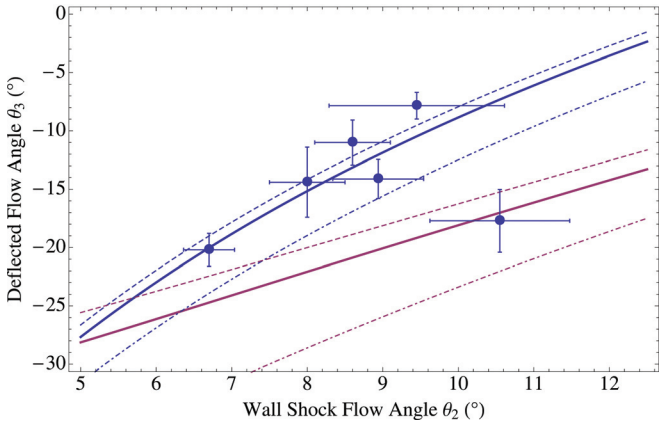

Fig. 9. (Color online) θ_2 vs. θ_3 measured in the October 2008 dataset and compared to (blue, solid) the radiative shock predictions and (red, solid) the nonradiative, purely polytropic predictions for for $V_r = 120, \gamma = 1.55$. The dashed lines show variation with γ in each case, from $\gamma = 5/3$ (above) to $\gamma = 1.2$ (below).

IV. CONCLUSIONS

We can construct, in analogy to the theory of oblique polytropic shocks, a theory of oblique radiative shocks. The radiative shock relations are constructed in media considered optically thin-upstream and optically thick-downstream of the shock, with realistic semianalytical equations of state providing ionization. The resulting oblique radiative shock relations are used to extend the graphical technique of shock polars in $(P/P_1, \theta)$ space, frequently used in the shock reflection literature, to include radiative systems. The resulting theory can address radiative shocks in a variety of interactions with both nonradiative polytropic shocks and walls. Analysis of the latter includes the effect of wall shocks launched by radiative vaporization of upstream wall material. These constructions are then used to describe multidimensional experiments including radiative shocks.

ACKNOWLEDGMENTS

This work is funded by the DOE NNSA-DS and SC-OFES Joint Program in High-Energy-Density Laboratory Plasmas by Grant No. DE-FG52-09NA29548, by the National Laser User Facility Program in NNSA-DS by Grant No. DE-FG52-09NA29034, by the Predictive Sciences Academic Alliances Program in NNSA-ASC by Grant No. DE-FC52-08NA28616, and by the DOE Stewardship Science Graduate Fellowship program.

[1]Y. B. Zeldovich and Y. P. Razier, *Physics of Shock Waves and High-temperature Hydrodynamic Phenomena* (Academic Press, New York, 1967).
[2]R. P. Drake, Phys. Plasmas **14**, 043301 (2007).
[3]F. H. Shu, *The Physics of Astrophysics: Gas Dynamics* (University Science Books, Sausalito, CA, 1992).
[4]S. Bouquet, R. Teyssier, and J. P. Chieze, Astrophys. J. Suppl. Ser. **127**, 242 (2000).
[5]R. P. Drake, *High-Energy-Density Physics* (Springer, Berlin, 2006).
[6]R. McClarren, R. P. Drake, J. E. Morel, and J. P. Holloway, Phys. Plasmas **17**, 093301 (2010).
[7]J. C. Bozier, G. Thiell, J.P. Le Breton, S. Azra, M. Decroisette, and D. Schirmann, Phys. Rev. Lett. **57**, 1304 (1986).
[8]S. Bouquet, C. Stehlé, M. Koenig, J.-P. Chièze,A. Benuzzi-Mounaix, D. Batani, S. Leygnac, X. Fleury, H. Merdji, C. Michaut, F. Thais, N.

Grandjouan, T. Hall, E. Henry, V. Malka, and J.-P. J. Lafon, Phys. Rev. Lett. **92**, 225001 (2004).
[9]P. A. Keiter, R. P. Drake, T. S. Perry, H. Robey, B. A. Remington, C. A. Iglesias, R. J. Wallace, and J. Knauer, Phys. Rev. Lett. **89**, 165003 (2002).
[10]D. Symes, M. Hohenberger, J. Lazarus, J. Osterhoff, A. Moore, R. Fustlin, A. Edens, H. Doyle, R. Carley, A. Marocchino, J. Chittenden, A. Bernstein, E. Gumbrell, M. Dunne, R. Smith, and T. Ditmire, High Energy Density Phys. **6**, 274 (2010).
[11]G. A. Rochau, J. E. Bailey, Y. Maron, G. A. Chandler, G. S. Dunham, D. V. Fisher, V. I. Fisher, R. W. Lemke, J. J. MacFarlane, K. J. Peterson, D. G. Schroen, S. A. Slutz, and E. Stambulchik, Phys. Rev. Lett. **100**, 125004 (2008).
[12]T. R. Boehly, D. L. Brown, R. S. Craxton, R. L. Keck, J. P. Knauer, J. H. Kelly, T. J. Kessler, S. A. Kumpman, S. Loucks, S. A. Letzring, F. J. Marshall, R. L. McCrory, S. F. B. Morse, W. Seka, J. M. Soures, and C. P. Verdon, Opt. Commun. **133**, 495 (1994).
[13]F. W. Doss, R. P. Drake, and C. C. Kuranz, High Energy Density Phys. **6**, 157 (2010).
[14]A. B. Reighard, R. P. Drake, K. K. Dannenberg, D. J. Kremer, M. Grosskopf, E. C. Harding, D. R. Leibrandt, S. G. Glendinning, T. S. Perry, B. A. Remington, J. Greenough, J. Knauer, T. Boehly, S. Bouqet, L. Boireau, M. Koenig, and T. Vinci, Phys. Plasmas **13**, 082901 (2006).
[15]F. W. Doss, H. F. Robey, R. P. Drake, and C. C. Kuranz, Phys. Plasmas **16**, 112705 (2009).
[16]S. Eliezer, A. K. Ghatak, and H. Hora, *Fundamentals of Equations of State* (World Scientific Publishing, Singapore, 2002).
[17]R. M. More, Technical Report No. UCRL-84991 Part 1, Lawrence Livermore National Laboratory (1981).
[18]D. Salzmann, *Atomic Physics in Hot Plasmas* (Oxford University Press, Oxford, 1998).
[19]C. J. Chapman, *High Speed Flow* (Cambridge University Press, Cambridge, 2000).
[20]R. Courant and K. O. Friedrichs, *Supersonic Flow and Shock Waves* (Interscience Publishers, New York, 1948).
[21]B. van der Holst, G. Toth, I. Sokolov, K. Powell, J. Holloway, E. Myra, Q. Stout, M. Adams, J. Morel, and R. Drake (2011), e-print arXiv:1101.3758v1.
[22]L. F. Henderson and R. Menikoff, J. Fluid Mech. **366**, 179 (1998).
[23]G. Ben-Dor, *Shock Wave Reflection Phenomena* (Springer, Berlin, 2007).
[24]H. S. Tsien and M. Finston, J. Aeronaut. Sci. **16**, 515 (1949).
[25]*General Theory of High-Speed Aerodynamics*, High Speed Aerodynamics and Jet Propulsion, Vol. 6. edited by W. R. Sears (Princeton University Press, Princeton, NJ, 1954).
[26]J. P. Cox and R. T. Giuli, *Principles of Stellar Structure* (Gordon and Breach, 1968).
[27]M. Hohenberger, D. R. Symes, J. Lazarus, H. W. Doyle, R. E. Carley, A. S. Moore, E. T. Gumbrell, M. M. Notley, R. J. Clarke, M. Dunne, and R. A. Smith, Phys. Rev. Lett. **105**, 205003 (2010).
[28]A. D. Edens, T. Ditmire, J. F. Hansen, M. J. Edwards, R. G. Adams, P. K. Rambo, L. Ruggles, I. C. Smith, and J. L. Porter, Phys. Rev. Lett. **95**, 244503 (2005).
[29]J. Grun, J. Stamper, C. Manka, J. Resnick, R. Burris, J. Crawford, and B. H. Ripin, Phys. Rev. Lett. **66**, 2738 (1991).